

# Design and Analysis of Deep Learning Method for Fragmenting Brain Tissue in MRI Images

Ting Yang, Jiabao Sun\*

School of Information and Electrical Engineering, Shaoxing University Yuanpei College, Shaoxing, Zhejiang, 312000, China

**Abstract**—An essential component of medical image processing is brain tumour segmentation. The process of giving each pixel a label is called image segmentation in order for pixels bearing the same label to share characteristics and help distinguish the target. A higher fatality rate and additional dangers can be avoided with early identification. It can be challenging and time-consuming to manually (man-made) segment brain tumours from the numerous MRI pictures generated during medical procedures in order to diagnose malignancy. This is the fundamental reason why brain tumour imaging has to be automated. The deep learning technique for the segmentation of brain tissue in magnetic resonance imaging (MRI) pictures was examined and enhanced in this work. Researchers are using deep learning techniques—convolutional neural networks in particular—to tackle the complex problem of biological image fragmentation object recognition. In contrast to traditional classification techniques that take in manually constructed qualities, convolutional neural networks automatically extract the required complicated features from the data itself. This solves a number of problems.

**Keywords**—Brain tumor; deep learning; neural networks; magnetic resonance imaging

## I. INTRODUCTION

Digital images are frequently utilised in image processing, and improved hospital healthcare services have been made possible in recent years by information technology and electronic health systems in the medical industry. When one or more malignant tissues in the brain grow abnormally, brain tumours result. There are two kinds of brain tumours: benign and malignant. A brain tumour is considered benign if the tumour tissues are growing uniformly and the cancer cells are dormant. A malignant tumour is one that spreads to all associated tissues if the cancerous tissues are non-uniform or if the cells are active, depending on the individual. Tumour location diagnosis is challenging due to the intricate structure and tissues of the human brain. Malignant tumours spread over the entire brain or spinal cord tissues, depending on when they are discovered. They do this by transferring diseased tissues to healthy tissues. Treatment for malignant tissues becomes more challenging and, in most circumstances, incurable, meaning the patient will eventually die from the disease as it spreads to additional regions. Thus, among the most important issues facing patients are early detection, type categorization, and infection rate.

With the development of new imaging techniques that make this information more accessible to doctors, radiation, surgery, or chemotherapy may be the best course of action. It follows that a patient's chances of surviving a tumour can be

greatly raised if the tumour is accurately discovered in its early stages. Under the effect of imaging techniques, fragmentation is employed to identify the tumour area [1], [2]. Texture, contrast, border, and colour are the different components that make up a picture. As previously stated, aberrant and non-uniform growth of brain tissues is the definition of brain cancer or brain tumour [3], [4]. Brain tumours are among the deadliest forms of cancer, although being relatively uncommon. Brain tissue cells are the source of cells seen in primary brain tumours, and they begin in the brain. An MRI of the patient's brain is one of the best methods for diagnosing brain tumours. This technique facilitates a simple first diagnosis by giving medical professionals vital information on the structure, size, and metabolism of the brain tumour. This type of imaging is a common way to look at and diagnose brain tissue.

The study employed a variety of segmentation techniques, including a histogram, neural network segmentation methods, physical model-based techniques, clustering algorithms, Mean-Shift algorithm, k-means algorithm, Fuzzy C-Means Clustering (FCM) Algorithm, and Expect maximisation algorithms, to diagnose and classify the type and size of brain tumours in patients [5], [6]. Based on the segmentation system performance, various segmentation techniques are compared. For improved segmentation, artificial intelligence and enough information are typically combined [7], [8]. Conversely, the deep learning approach has shown the best results.

Abd-Ellah et al. reviewed the diagnosis of brain tumours using MRI scans in 2019 [9]. Additionally, the Support Vector Machine's (SVM) and Ecoc's error correction output codes are used to attain accuracy in the classification stage. PCA is used for feature extraction and selection in DWT machine learning. The collected features are classed using a seven-layer dynamic neural network (DNN) [10]. Terms and titles like CNN architecture, inverted graphics network, deep neural network, deep belief network, and so on are used in image processing technology; CNN architecture is the most commonly used word. Convolutional layers are typically used in the CNN architecture's feature extraction layer and input layer. The suggested method was proposed by Mohan et al. (2018) in three primary steps: CNN classification, post-processing, and pre-processing. Because CNN architecture performs so well in brain image recognition, medical professionals and researchers are using it more frequently than they used to because it is faster and more accurate than other methods. [11, 12]. A faultless network architecture is made possible by the CNN approach, which directly learns the difficult and complicated aspects of brain MRI images to aid in feature extraction and reduction. CNN receives brain MRI image excerpts as input,

and uses Neutral Density (ND) filters to extract complicated characteristics. The benefits of CNN architecture have been covered thus far; however, there are drawbacks to this approach as well, including high training computational costs, data consumption, and challenging hidden-layer complicated architecture design. It has also looked at the difficulties and issues that other studies have had when reporting the data, the type of tumour, and the algorithms' performance standards utilising the sensitivity, precision, and accuracy criteria. Based on the research and studies conducted, it is recommended that greater focus be placed on the identification, location, segmentation, and algorithm validation of brain tumours using magnetic resonance imaging.

When a brain tumour reaches an advanced stage, it can be difficult to diagnose it quickly. Magnetic resonance imaging is often chosen to improve the outcome of brain tumour diagnosis. It is exceedingly challenging to identify a tumour more accurately without harming healthy tissue. A new method for using magnetic resonance imaging (MRI) to diagnose brain tumours is presented in order to fix the flaws [13], [14]. As previously shown, early diagnosis of brain tumours can greatly aid patients in their recovery, contingent upon the nature and degree of metastasis. In the clinic or hospital, manually evaluating the numerous magnetic resonance imaging (MRI) scans that are generated on a regular basis is a challenging procedure. Thus, computer technologies should be employed for fast and accurate early diagnosis of brain tumours. Three key components are involved in diagnosing brain tumours using MRI images: segmentation, classification, and tumour diagnosis. Studies show that the majority of works in recent years have concentrated on the application of conventional learning machines. More precise techniques have been used recently by researchers; these are also used to find brain tumours. In general, this article's main theme gives a summary of both the development processes for new deep learning approaches for diagnosing brain cancer and traditional machine learning techniques.

The primary goals of the research presented in this paper are to provide an enhanced approach for brain segmentation, assess the effectiveness of the suggested approach, and review and compare the current approaches for brain tumour segmentation. The article's overall structure is set up so that the Section II provides a summary of the fundamental ideas and earlier approaches used in this area. The recommended dataset is introduced in the Section III, while the recommended approach is offered in the second portion. The steps for the study method are presented in the Section IV. The suggested approach is tested, its outcomes examined, and it is contrasted with alternative segmentation techniques in the Section V. The suggested algorithms are concluded and summarised in Section VI.

## II. PROPOSED METHODS

An enhanced strategy built on the deep learning technique is provided in this section. Compared to previous methods, the suggested method offers a higher sensitivity and accuracy. Neural networks can be used to implement the suggested method. Deep learning is one of the subgroups of machine learning. According to a set of techniques, deep learning

attempts to model high-level abstract notions in the data by using a deep graph with numerous processing levels made up of several linear and non-linear transformation layers [15], [16]. The study of neuronal behaviours in the human brain provides the learning structure with its primary purpose [17]. Models like deep neural networks, sophisticated neural networks, and deep belief networks have advanced well in the domains of image and natural language processing [18], [19]. In actuality, the study of novel artificial neural network techniques is referred to as deep learning. Deep learning can be used to meet the issues of avoiding the drawbacks of traditional machine learning methods [20], [21]. In several fields of medical image analysis, including computer-aided diagnosis, in-depth learning is becoming more and more common [22], [23]. As was previously noted, one of the subcategories of machine learning technology is the deep learning algorithm, which looks for many levels of distributed input data. The paper introduces a novel approach for segmenting tumour locations using a mix of artificial neural network and K-means fuzzy algorithm [37]. The process comprises of four stages, namely denoising, feature extraction and selection, classification, and segmentation. Initially, the preprocessed image is eliminated utilising the Wiener filter, subsequently followed by the extraction of significant GLCM features from the images. Subsequently, deep learning techniques were employed to categorize abnormal photos from normal images. Ultimately, the tumour region is segmented independently by subjecting it to the K-Means fuzzy algorithm. The proposed segmentation strategy is tested on the BRATS dataset and achieves an accuracy of 94%, a sensitivity of 98%, a specificity of 99%, and a Jaccard index of 96%. To address these issues, a fresh and enhanced deep learning model for image segmentation based on the cascaded regression (DLCR) technique is put forth. The fully convolutional neural network (FCNN) method is used in the suggested method to pre-process magnetic resonance imaging (MRI) pictures using the normalisation method. The data is then reduced and the matching feature from each feature vector is obtained through feature extraction using the Gaussian mixture model (GMM). Next, our suggested approach was contrasted with the existing techniques, which include the predictive machine learning model (MLPM), deep learning framework (DLF), and extreme learning machine local receiving fields (ELM-LRF). According to the findings, the suggested DLCR approach outperforms the current techniques in terms of sensitivity, specificity, recall ratio, precision ratio, peak signal-to-noise ratio (PSNR), and root mean square error (RMSE) [38].

These techniques are often divided into four groups: auto encoders, convolutional neural networks, sparse coding, and restricted Boltzmann machines (RBMS). Unlike human feature extraction in classical learning methods, machine learning technology may extract complex stages from their learning abilities. Through training, they get more acceptable findings in vast data sets. The fast rise in GPU processing capacity has enabled the creation of cutting-edge deep learning methods. Deep learning algorithms have been trained against picture alterations using millions of photos and resistance [24], [25].

An artificial neural network that resembles the structure of the human brain and is capable of carrying out mathematical

operations is called a deep learning algorithm. However, technological developments have given rise to methods for optimising traditional neural networks [26]. A multi-layer neural network with numerous hidden layers and free parameters does deep learning [27]. One of the most significant deep learning techniques is convolution neural networks, which effectively train several layers. This is one of the most popular and highly effective ways. The convolution layer, pulling layer, and fully connected layer are the three primary layers that make up a CNN network in general. Various layers carry out various functions. There are two steps in a convolutional neural network: the feed stage and the backpropagation stage for training.

Convolution is applied to each layer of the image after the point between the input and each neuron's parameters is multiplied in the first step. This step involves feeding the network input and then computing the network's output. The network error is computed and the network parameters are set using the output outcome. In order to calculate the error rate, compare the network output with the right response using a loss function. The post-publication stage starts in the following step, based on the computed mistake amount. Using the loss function, the network's output is compared to the right response to determine the error rate. The post-release stage starts in the following phase, depending on the quantity. This phase computes each parameter's gradient using the chain law. Every parameter has an effect on the network, according to the error made on each parameter based on the methodology. The feeding step is forward once the network has been modified and the parameters have been updated. Eventually, following numerous iterations of these procedures, the network's training is complete.

#### A. CNN Network Layers

Convolutional neural networks, in general, are neural networks with particular, hierarchical rules in which a number of fully connected layers come after the convolutional layers and the pulling layers. The convolution layer is one of the CNN layers. In these layers, the CNN network solves the middle feature map and the input picture using several cores, which results in distinct features in Fig. 1. There are three advantages to convolution operations: stability, immutability with regard to object relocation, local connectedness, and a significant reduction in the number of parameters.

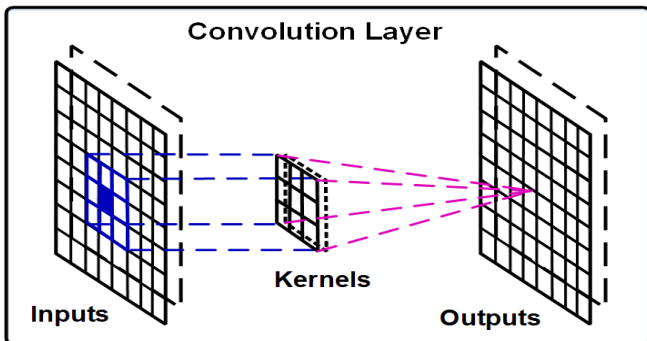


Fig. 1. Convolution layer performance.

The Pooling layer is the subsequent CNN layer. Pooling layers, which are frequently placed after a convolutional layer,

can be used to reduce the size of the feature map and network parameters. Convolution layers and other pooling layers are resilient against displacement because they incorporate nearby pixels into their computations. The most popular pooling layer implementations make use of the max (max pooling) and average (average pooling) functions. It accelerates convergence, enhances generalisation, and produces a well-chosen set of fixed features. Fig. 2 displays a max-pooling result.

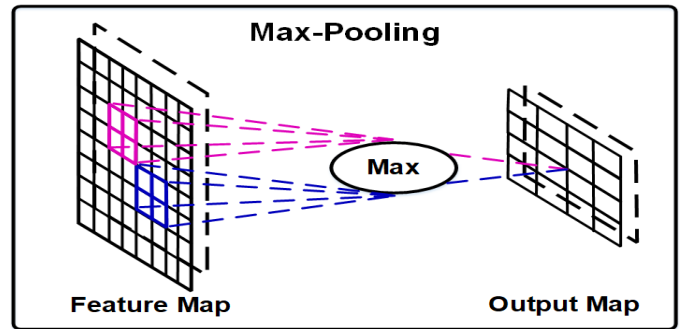


Fig. 2. Max-pooling performance.

The fully linked layer is the final layer of CNN. As seen in Fig. 3, there are fully linked layers following the final polishing layer, each of which is connected to the neurons in the layer before it. On the other hand, about 90% of the parameters of a CNN network are made up of fully linked layers, which are likewise conventional.

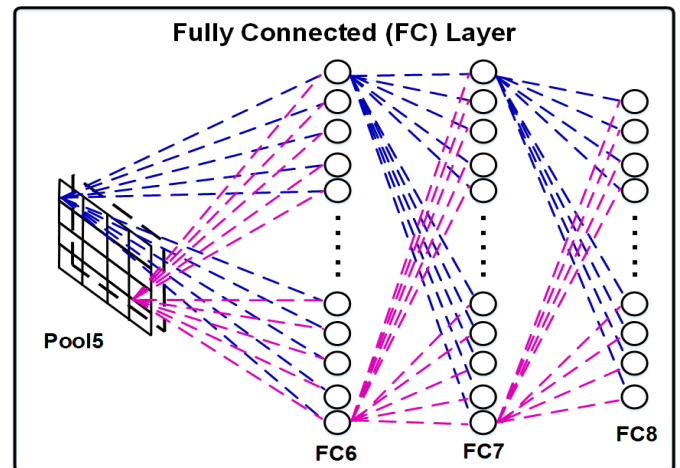


Fig. 3. Fully connected layers performance.

This kind of layer's main problem is its excessive number of parameters. As a result, there is a significant processing cost that needs to be covered by training. Therefore, cutting back on connections and eliminating these layers entirely using various techniques is a popular technique that yields good results.

#### B. Enhanced Neural Network Capabilities

The advantage of deep learning over surface learning is the ability to build deep architectures with higher data volumes and higher abstract information transmission. However, overfitting may become a problem if a lot of new parameters are included. A plethora of regularisation techniques have been introduced recently to address overfitting and enhance network

performance. Note that not every method covered in this section is unique to neural networks. This implies that various methods, such as the dropout method, can be used with conventional artificial neural networks.

1) *Deep learning dropout*: The purpose of this approach is to prevent over-coverage. Each neuron in the network is either retained with a probability of  $p$  or eliminated with a probability of  $p-1$  at each training stage. Eventually, just a smaller network is left. An expelled node's input and output edges are also eliminated. At that point, the data will only be used to train the smaller network. Next, the removed nodes are removed from the network and then added back in with their original weights. A comparison between the networks is shown in Fig. 4.

Drop Connect is a well-liked variation of Dropout that drops weights at random rather than activation values. Research has demonstrated that, albeit more slowly, this approach can regularly outperform the Dropout method in a variety of common benchmark categories.

2) *Deep clustering in deep learning*: Without any prior knowledge of different factors like feature selection, distance criteria, or clustering techniques, the goal of clustering is to group comparable data points. One deep learning algorithm is deep clustering. Two-dimensional non-linear data representations from the data set are employed for learning. Quantization of deep neural networks requires network loss. Deep clustering techniques now in use can be generally classified into two groups. After learning a representation that jointly optimises learning and clustering, a two-step challenge is implemented. The first class of algorithms makes use of sophisticated unsupervised learning frameworks and methodologies directly. An additional set of algorithms simulates a classification error in monitoring by attempting to precisely characterise a clustering failure.

3) *Data redundancy in deep learning*: The utilisation of redundant data results from the redundancy of data generated when CNN is utilised for object detection. Forecasts may benefit from the addition of new data, which also improves the data's quality and accuracy. This can be used to decrease interference and expand training set sizes. [28, 29]

4) *In deep learning, auto encoder and deep auto encoder*: A neural network that has been trained to replicate its input to its output is called an autoencoder. Neural networks whose input and output are identical are an artificial neural network type that is used to encode effective learning data in an unsupervised manner. They function by first compressing the input into a representation of hidden space, from which the output is then rebuilt. An autoencoder aims to encrypt a dataset, usually with the purpose of reducing dimensionality by conditioning the network to reject spurious signals. Fig. 5 depicts an autoencoder's full workflow. You train an autoencoder to re-encode your input  $X$ , as opposed to training the network to anticipate the target value  $Y$  for the input  $X$ . During this procedure, the auto-encoder is optimised by minimising the update error.

Hinton [28] introduced the deep autoencoder, which is still being researched extensively in current studies. As previously noted, a backpropagation process, like the gradient approach, is used to train the autoencoder. Ignoring the benefits, this model's significant drawback becomes apparent when an error happens, and these layer flaws can cause the model to become extremely inefficient. The network reconstructs the training data average as a result of this error. This problem can be effectively solved by pre-training the network with initial weights, which comes close to the ultimate solution. Simultaneously, several auto-encoders are available that promise to retain representations for an extended period of time due to continuous changes in input. The autoencoder is compelled by full representation learning to extract the most important features from the data.

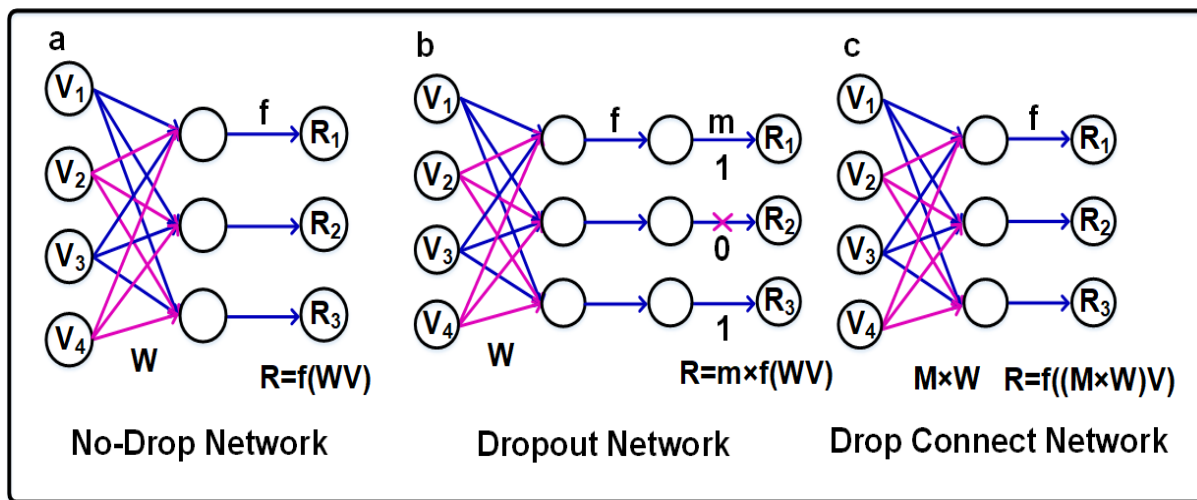


Fig. 4. Comparison between the networks.

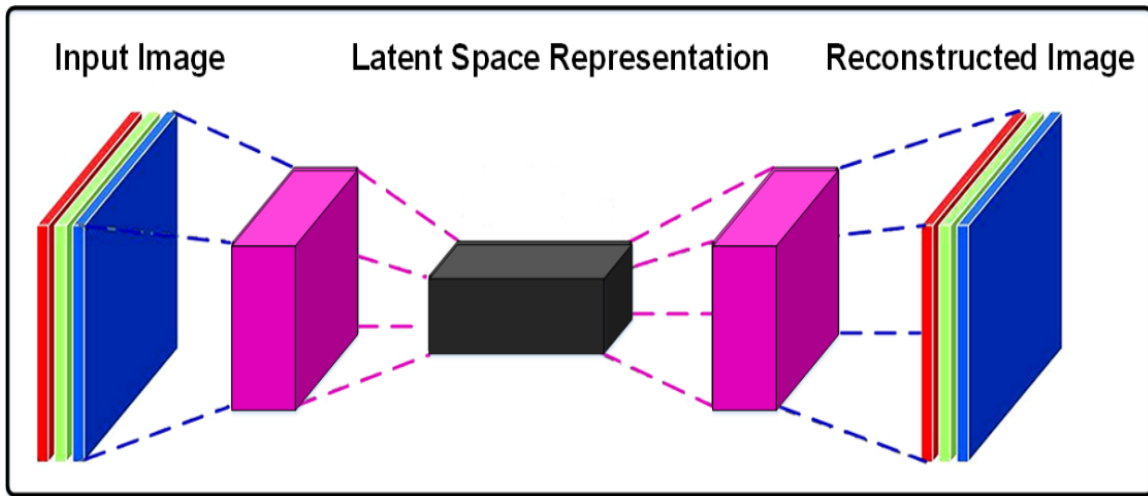


Fig. 5. The autoencoder's general process.

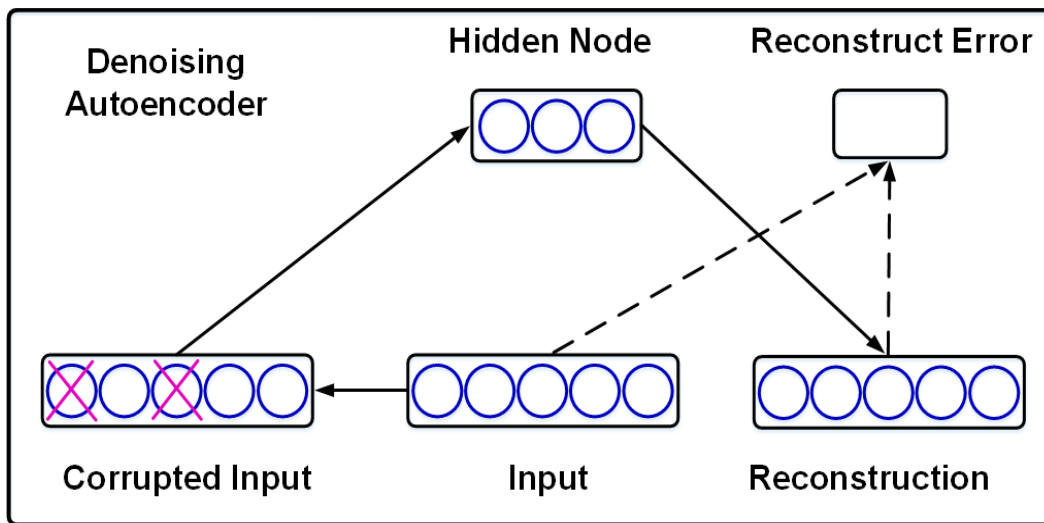


Fig. 6. Denoising autoencoder.

5) *Denoising autoencoder in deep learning:* In Fig. 6, the DAE procedure is displayed. (DAE) is a power-boosting model known as an automatic denoising encoder. Vincent presents this model, which is able to discern between the accurate input and the tampered version. Put another way, have the model see the input distribution's structure.

In actuality, this task's objective is to either eliminate or clean up the contaminated input. The depiction of higher levels that are comparatively resistant to corrupt inputs and the extraction of characteristics with a relevant structure in the input distribution are the two linked hypotheses of this technique. Its ability to correctly recover from a damaged version is one of its excellent features, and it is noise-resistant.

### C. Network in Network (NIN) and Activation Functions

Fully linked layers are used for image processing after a series of layers and aggregation layers are used to extract features from spatial structures. The primary idea behind it is to substitute a perceptron neural network (many fully connected layers with non-linear activation functions) for the

convolutional layer and learn its parameters from the data. In this sense, non-linear neural networks take the place of linear filters. This technique produces superior picture categorization results. It is in charge of the data's non-linear transformation. The modified linear unit (ReLU) is computed in Eq. (1).

$$F(x)=\max(0, x) \quad (1)$$

It has been discovered that these functions outperform hyperbolic tangent functions or classical functions in terms of training speed [30], [31]. On the other hand, applying a constant 0 can harm the flow gradient and the subsequent weight adjustment [32], [33]. Using a variable named Leaky Rectified Linear Unit (LReLU), which adds a tiny slope to the performance's negative side, we adjust to these constraints. Eq. (2) is used to calculate this function.

$$F(x)=\max(ax, x) \quad (2)$$

The activation function is among the most often used (ReLU). The ReLU non-linear unit's job is to clip any negative input value in the data to zero, reducing it, and then taking the positive input values as the output [34], [35].

### III. DATA SET

We utilised the publically accessible brain tumour dataset from Figshare [4] to examine and assess our suggested methodology, employing various convolutional neural network designs. Cheng developed it in 2017. The dataset consists of 3064 brain MRI slices obtained from 233 people. It encompasses three types of brain tumours:

The total amount of images for meningioma is 708, for pituitary it is 930, and for glioma tumour it is 1426. The dataset is accessible to the public via the Figshare website in the ".mat" format, which is compatible with MATLAB. Each MAT-file consists of a structure that includes a patient ID, a distinctive label indicating the type of brain tumour, picture data in a  $512 \times 512$  format represented as unsigned 16-bit integers, a vector providing the coordinates of discrete points that define the tumour perimeter, and a binary mask image representing the ground truth. Fig. 7 shows the eight examples of database images.

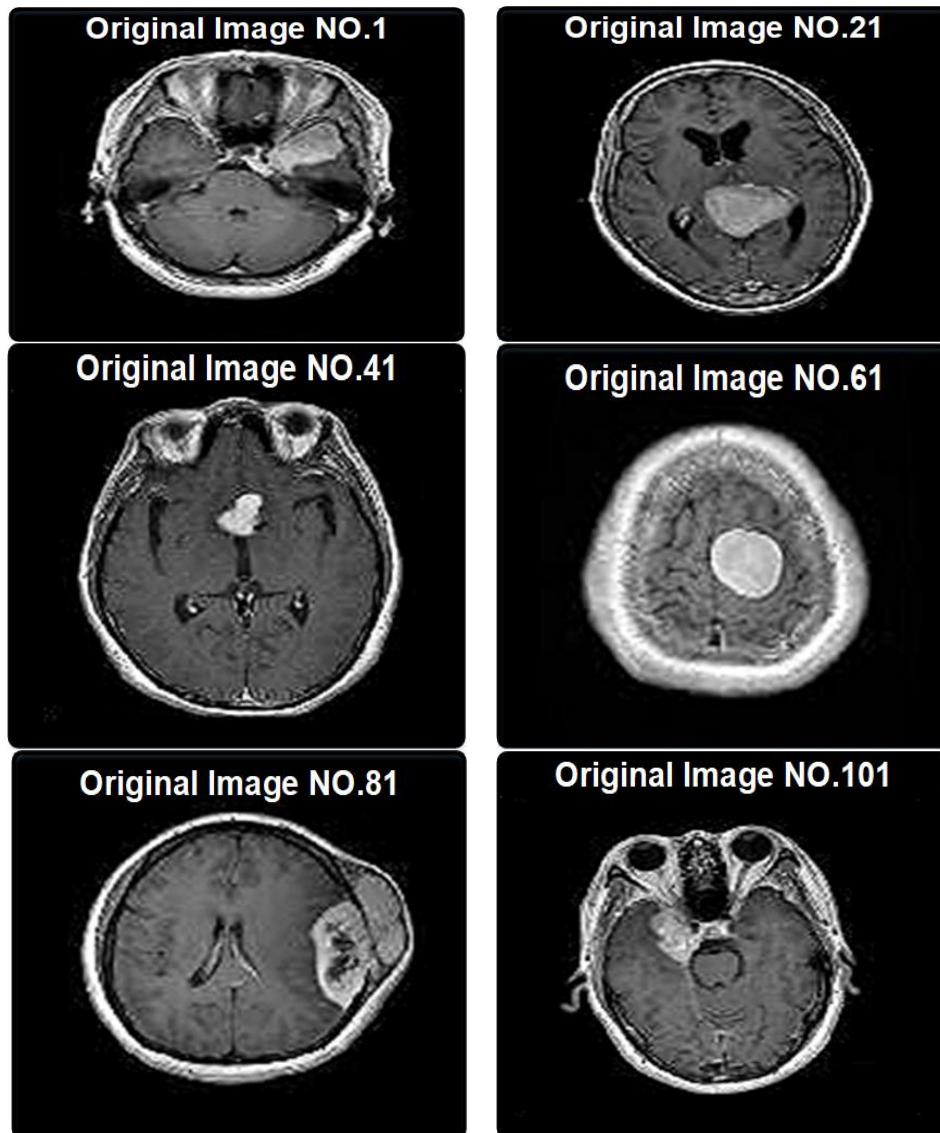
The enhanced deep learning algorithm's pseudo-code is presented in the text below.

An overview of CNN architecture is presented in Fig. 8.

Algorithm 1: Improved Deep Embedded Clustering

**Input:** Input data:  $X$ ; Number of clusters:  $K$ ; Target Distribution update interval:  $T$ ; Stopping Threshold:  $\delta$ ; Maximum iterations:  $MaxIter$ .  
**Output:** Autoencoder's weights  $W$  and  $W'$ ; Cluster centers  $\mu$  and labels  $s$ .

- 1 Initialize  $\mu, W'$  and  $W$  according to Section 3.1.
- 2 **for**  $iter \in \{0, 1, \dots, MaxIter\}$  **do**
- 3 **if**  $iter \% T == 0$  **then**
- 4 Compute all embedded points  $\{z_i = f_w(x_i)\}_{i=1}^n$
- 5 update  $P$  using (3), (4) and  $\{z_i\}_{i=1}^n$ .
- 6 Save last label assignment:  $S_{old} = s$ .
- 7 Compute new label assignment  $s$  via (14).
- 8 **if**  $\text{sum}(S_{old} \neq s) / n < \delta$  **then**
- 9 **Stop training.**
- 10 Choose a batch of sample  $S \in X$ .
- 11 Update  $\mu, W'$  and  $W$  via (11), (12) and (13) on  $S$ .



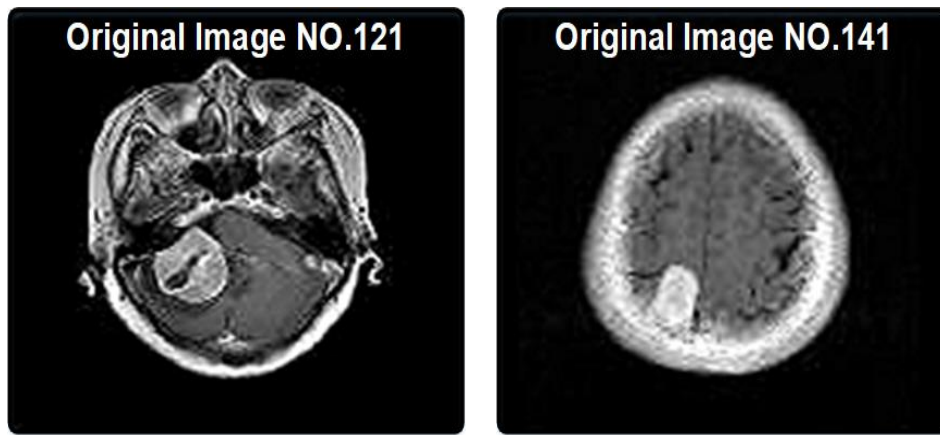


Fig. 7. The eight examples of database images.

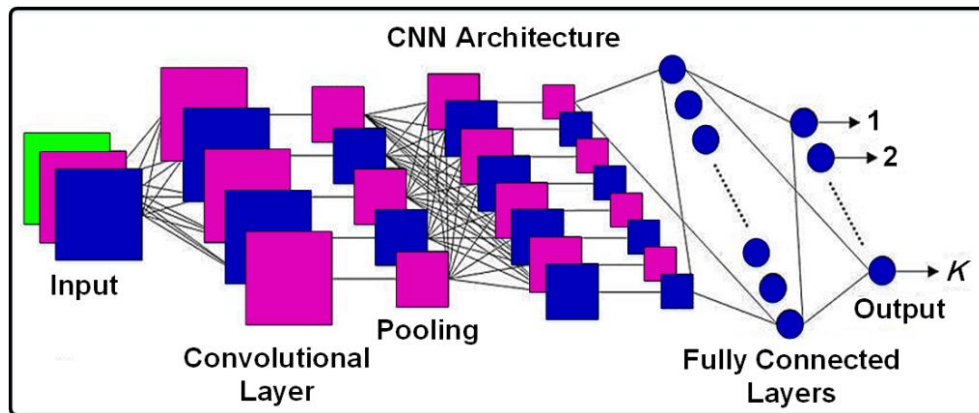


Fig. 8. CNN architecture.

#### IV. STUDY METHOD STEPS

Early diagnosis, therapy, and follow-up are made possible by having an effective brain tumour detected by multimodal imaging as soon as possible [36]. In some social networks, deep learning algorithms have quickly taken the lead in medical picture analysis. We investigate deep learning applications in object detection, segmentation, recording, and image classification. The proposed deep learning models work well for brain tumour segmentation and provide very accurate results. The suggested models can also assist medical practitioners in shortening the time needed for diagnosis. The goal of this research is to create a fully automated model for MRI brain tumour segmentation that operates without the need for human intervention. Instead of having multiple boxes (or networks) from input to output, a single grid is used in this deep learning model's proposal. Deep-end learning typically uses a neural network in place of the numerous processing stages that standard machine learning techniques typically call for. In order to get the most out of each layer before going on to the next, we construct this final model. When treating malignant tumours, deep learning models are employed. These tumours can arise anywhere in the brain and have four unpredictable characteristics: varying sizes, forms, and contrast. Therefore, convolutional neural networks are the best option for machine learning.

##### A. Pre-processing

To get better results, adjustments to the photos are required. Understanding, processing, and picture analysis are some of these adjustments. These modifications enhance image processing systems to enable them to carry out tasks more quickly and accurately. Pre-processing, picture quality enhancement, image conversion, categorization, and image analysis are the primary procedures that raise the efficiency of these systems, in that order. These techniques involve analysing images for certain goals, with computer-generated mathematical equations simulating irregular human visual features. Computer vision is the scientific image analysis used in many areas of engineering, health, imaging, security, and astronautics. Modern digital technology is able to operate multidimensional switches and many parallel computers thanks to systems derived from simple digital circuits.

One of the things like image processing, picture analysis, and image perception is the goal of these modifications. Since the majority of remote sensors store their data digitally, digital processing is eventually needed for all picture interpretation and analysis. In order to allow further interpretation and analysis, digital image processing may comprise a variety of processes, such as alteration, digital optimisation, data formatting, or even computer goals automation and automatic properties. To carry out this procedure, the data must be in a format that is appropriate for physical storage.

Four categories comprise the most often utilised processing procedures in image analysis systems: pre-processing, image enhancement, image transformation, image analysis, and classification. These procedures fall under the general category of radiometric or geometric adjustments and are typically grouped prior to the primary picture analysis and information extraction. To get an accurate picture of the radiation that the receivers are receiving, radiometric corrections entail adjusting data for undesired noise and anomalies in the receivers. The purpose of geometric corrections is to simplify the image and translate it into actual coordinates on the surface of the earth.

The procedures used in the Image Enhancement category are only intended to raise and enhance the image's resolution in order to provide a better understanding of the image. These acts are hypothetically comparable to the preceding category in picture transmission. However, this group involves the combined processing of data acquired from various spectral bands, in contrast to this group, which pertains to only one data channel. The original bands are combined with mathematical operations (addition, subtraction, multiplication, and division) to create new images that are more readable or have better qualities. Pixel classification and analysis aim to identify and characterize data pixels. The process of classifying assigns each pixel in an image to a group or theme based on the statistical characteristics of its floating values. It is typically applied to multi-channel data groups. There are two main approaches to this: supervisor-free and supervisor-involved.

#### B. Image Transformation Color to Gray

Three colors green, blue, and red combine to form the most common colour model in computer graphics. These three elements can combine to give a total of 16581375 distinct colours. In computer graphics, this colour model is referred to as RGB. Apart from the RGB colour model, there exist various additional models that display colours differently, including CMYK, HSI, HSV, and Grayscale. We are particularly interested in the Grayscale colour model in the interim. Because a grayscale image will do in the majority of applications, and a colour image is not necessary. Generally speaking, the grey image is referred to as the black and white image (of course, calling something grey instead of black and white is incorrect; this is just being clarified). Three matrices, one for each of the colours red, green, and blue in the image, make up an RGB image. Three matrices are created by mixing the values from the appropriate verses to display the image on the screen. For the majority of applications, a grayscale image will do; a colour image is not necessary. When the values of the R, G, and B components of a pixel are the same, the pixel will have a grey value. In accordance with this concept, he utilised Eq. (3) to grayscale input images that are RGB.

$$S_{_R(x,y)}=S_{_G(x,y)}=S_{_B(x,y)}=\frac{[R(x,y)+G(x,y)+B(x,y)]}{3} \quad (3)$$

where, R, G, and B are the matrices representing the red, green, and blue components of the input image, and S\_X are the components of the output image.

#### C. Median Filter

Among the non-linear filters is the median filter. Signals and noise in images are captured using this filter. Picture noise

refers to background and other picture detections. For instance, you have to take a picture using one of the filters like the median noise filter—before you can identify a corner. When processing images, the median filter is frequently used. It is also impossible to overlook the median filter's application in signal processing. The median filter is utilised in blood pressure monitors, EEG systems, and radiography systems, among other specialised applications. We can list median and fashion filters as examples of non-linear filter types. The median filter is a low-pass filter that uses a face neighbourhood to sort the neighbourhoods in ascending order before sorting the middle element of the numbers to replace the centre pixel. It should be mentioned that noise from salt and pepper can be eliminated using the mid-pass filter.

#### D. SOBLE Filter

There are three ways to convert a colour image to grayscale: edge features, edge detection, and image edging techniques. As using image edging techniques, the light intensity dramatically changes as points are marked in the image for edge identification. Changes in image properties are indicative of major changes in environmental factors. Image processing and feature extraction researchers are studying edge identification. The boundary in edge detection is found between regions of the grey surface with comparatively distinct characteristics. The fundamental idea behind the majority of edge detection techniques is the computation of a local derivative operator. It should be noticed at this point that the edge—the change from dark to light—is modelled as a gradual, rather than abrupt, grey surface change. This model demonstrates how sampling typically causes the borders of digital images to become slightly blurry.

#### E. Image Binary Threshold

A threshold value must be used to establish the threshold when converting a grayscale image to a binary image. Pixels that are less than the threshold are assigned a value of 0, while those that are less than the threshold are assigned a value of 1 or 255. Thresholding an image can be done in various ways. They can be broadly separated into the five sections listed below. 1) Histogram-based techniques have been examined, including the analysis of the peaks, valleys, and curvatures of the smoothed histogram. 2) Clustering-based techniques, in which a grayscale image is divided into foreground and background. 3) Entropy-based techniques: these techniques determine the threshold based on the intersection of the two classes in the image as well as the background and background entropy distributions. 4) Object property-based methods: these determine the appropriate threshold by calculating the degree of similarity between the image and a binary and grayscale scale. 5) Location-based techniques: the desired threshold is computed using a higher-order probability correlation or distribution between pixels.

#### F. Tumor Detection

Automatically detecting and extracting a portion of a tumor from a brain image is a challenging and complex mission for doctors and physicians.

## V. DISCUSSION

Systems for detecting brain tumours are employed in numerous sectors. One of the main objectives of this field's study is to use deep learning to develop a solution that complies with the guidelines and standards of brain tumour diagnosis systems, hence improving the precision of medical specialists. MATLAB software is used to perform the simulations. Its accuracy, precision, and sensitivity are higher than those of the approaches offered, based on the evaluation findings. The research methodology was covered in the previous section; the simulation findings are reported in this

section. Fig. 9 shows the original image (a) and the image with a balanced histogram (b). Histogram balancing is the initial stage of image processing that enhances image quality.

The histogram in Fig. 10(a) shows the image prior to balancing and in Fig. 10(b) is the image following balancing. The horizontal axis of the histogram represents the colours, while the vertical axis represents the quantity of pixels in each colour. When using image histogram balancing, the image extends between 0 and 255 if the colour is between 0 and 100 when balanced.

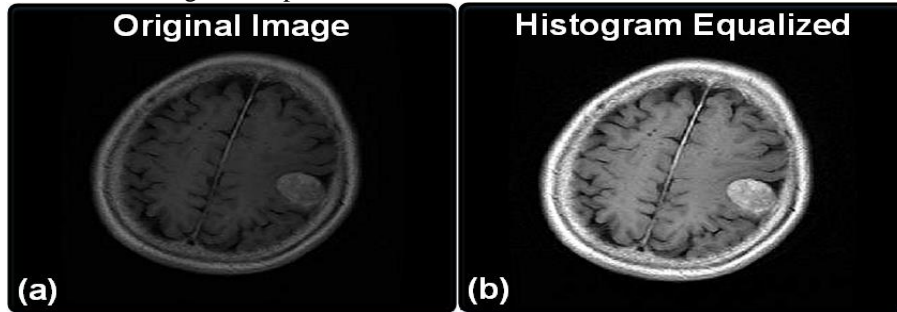


Fig. 9. (a) Original image, (b) Histogram balancing.

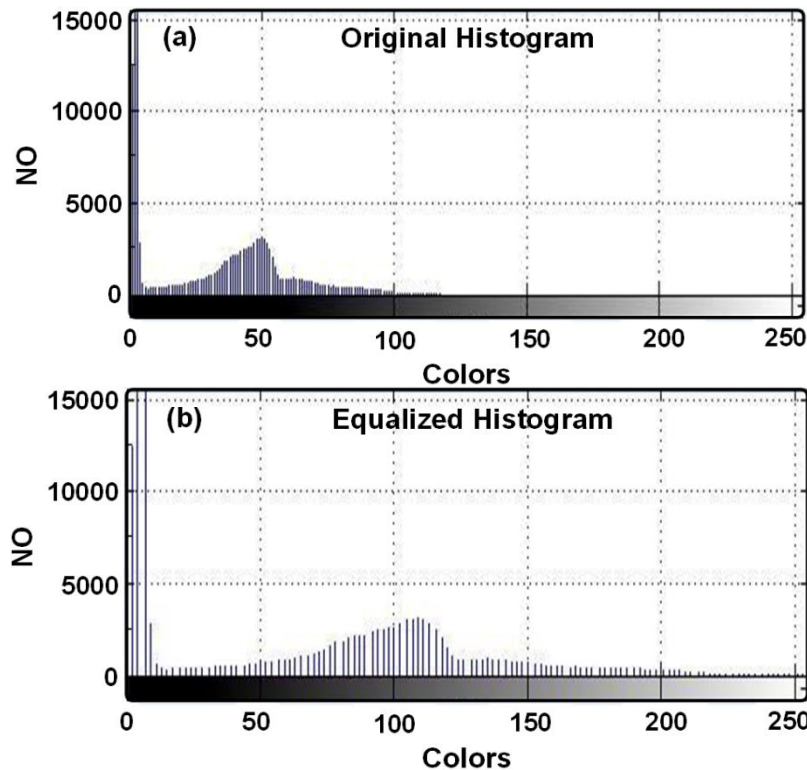


Fig. 10. Image histogram, (a) Original, (b) Equalized.

In Fig. 11, the median filter operation is performed on the main image. To improve those pixels that is not of good quality. It is actually to improve the quality of images.

Fig. 12 shows the Sobel image and the original image is binaries in Fig. 13. In order to isolate the objects in a digital image from their backdrop and analyse them, the image is first

converted to a binary image. This produces a binary image that is less in volume than the original image.

In the part of the images that are interconnected, the box is drawn with red lines around it by writing the program, as shown in Fig. 14. In other words, it actually features extraction.

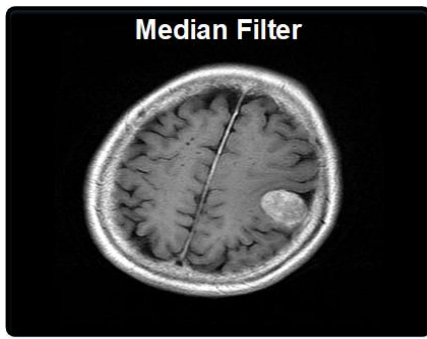


Fig. 11. Median filter.

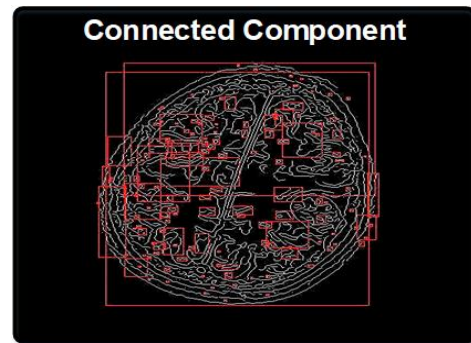


Fig. 14. Connected component.

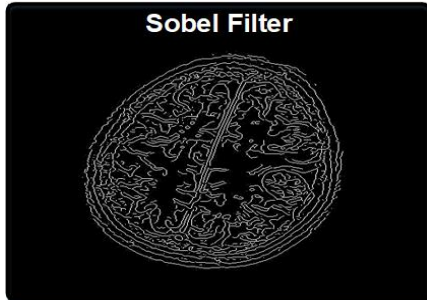


Fig. 12. Sobel image.

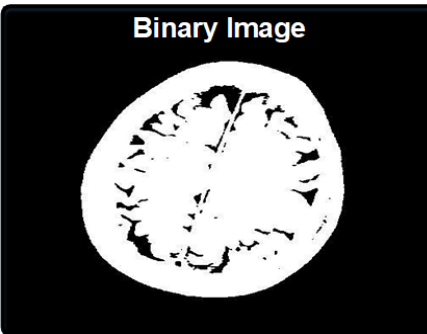


Fig. 13. Binarization.

#### A. Tumour Detection

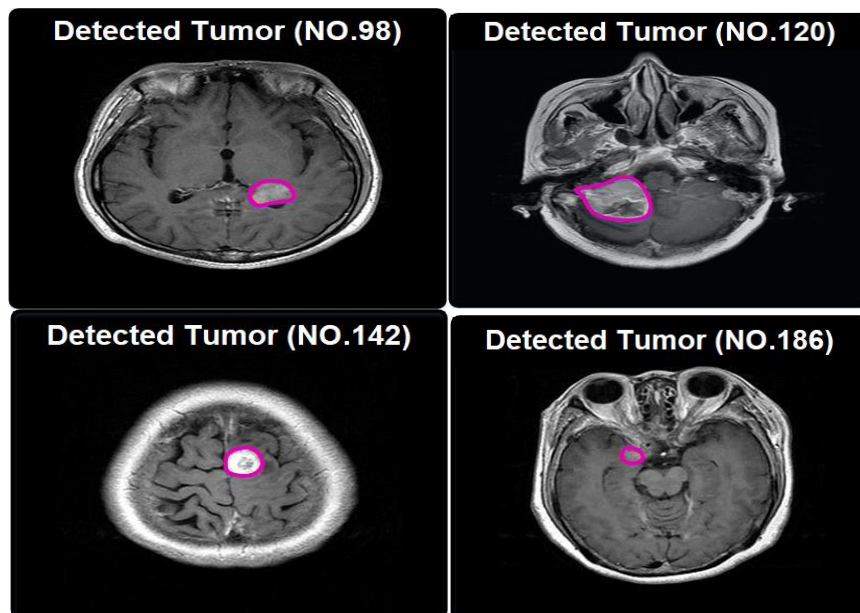
A comparison of the results with other approaches is made, taking into account various circumstances to demonstrate the effectiveness of the suggested method. Simulated approaches are identical in terms of conditions and evaluation parameters. Lastly, graphs are used to plot and analyse the simulation findings.

Each of the 766 data points is put in for loop in the MATLAB programme with the intention of being worked on. Following the use of the enhanced DEEP LEARNING algorithm to identify tumour sites in the output photos, these 14 sample images are displayed. Brain tumours are depicted in these pictures as pink in Fig. 15.

#### B. Evaluation Results

There are four sections to the evaluation results. 1) Positives that are accurately identified as true positives (TP). 2) False positives (FP), or negatives with a valid diagnosis. 3) Mistaken positives that are actually true negatives (TN). 4) Misdiagnosed negatives, or false negatives (FN). The assessed positive characteristics for simulating the first through sixth scenarios using various techniques are displayed in Table I.

Table II shows the evaluated negative parameters to simulate the seventh to twelfth scenarios for different methods.



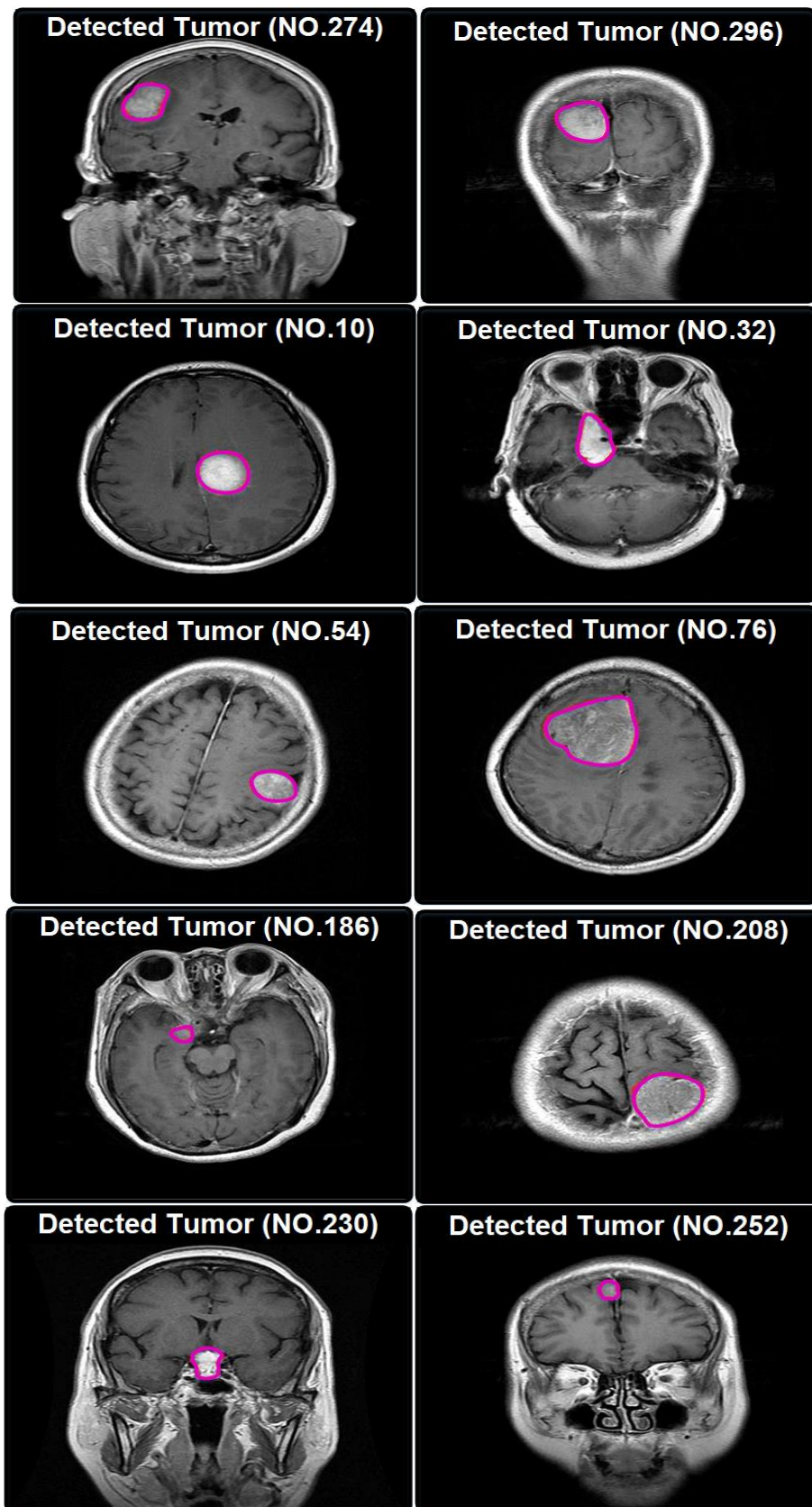


Fig. 15. Tumor detection results.

TABLE I. POSITIVE EVALUATION PARAMETERS

Scenario	Method	Accuracy (%)	TP Ratio (%)	Precision TP (%)	Recall TP (%)	F-Measure (%)	Precision (%)
1	proposed method	95	-	-	-	-	-
	Neural network	90					
	SVM	79					
	correlation	74					
	Euclidean	58					
2	proposed method	-	98	-	-	-	-
	Neural network		96				
	SVM		95				
	correlation		94				
	Euclidean		87				
	differential		48				
3	proposed method	-	-	93	-	-	-
	Neural network			74			
	SVM			69			
	correlation			66			
	Euclidean			63			
4	proposed method	-	-	-	98	-	-
	Neural network				96		
	SVM				95		
	correlation				94		
	Euclidean				48		
	differential				40		
5	proposed method	-	-	-	-	95	-
	Neural network					90	
	SVM					79	
	correlation					74	
6	proposed method	-	-	-	-	-	95
	Neural network						90
	SVM						40

TABLE II. NEGATIVE EVALUATION PARAMETERS

Scenario	Method	Accuracy Total (%)	TN Ratio (%)	Precision TN (%)	Recall TN (%)	Accuracy TN (%)	F-Measure TN (%)
1	proposed method	93	-	-	-	-	-
	Neural network	69					
	SVM	66					
	correlation	63					
2	proposed method	-	60	-	-	-	-
	Neural network		52				
	SVM		37				
	correlation		30				
3	proposed method	-	-	66	-	-	-
	Neural network			62			
	SVM			60			
	correlation			58			
	Euclidean			55			
	differential			24			
4	proposed method	-	-	-	60	-	-
	Neural network				52		
	SVM				49		
	correlation				46		
	Euclidean				22		
5	proposed method	-	-	-	-	66	-
	Neural network					62	
	SVM					60	
	correlation					58	
	Euclidean					24	
	differential					22	
6	proposed method	-	-	-	-	-	60
	Neural network						52
	SVM						24

TABLE III. RELATIONSHIPS RELATED TO THE EVALUATION PARAMETERS

-	Reference Standard Stroke	Reference Standard No Stroke	-
Self-report Stroke	(TP)	(FP)	$PPV=TP/TP+FP$
Self-report No Stroke	(FN)	(TN)	$NPV=TN/FN+TN$
-	$Sensitivity=TP/TP+FN$	$Specificity=TN/FP+TN$	-

In Table III, the relationships related to the evaluation parameters are calculated.

1) *Positive evaluation results:* The accuracy diagram, which compares the suggested method with the neural network, SVM, correlation, and Euclidean methods in Fig. 16, shows the green colour of the suggested method, the red colour of Euclidean, the black colour of correlation, the blue colour of the support vector machine, and the purple colour of the neural network. The training data percentage in the data set is shown by the horizontal axis in this image, and the accuracy %, which ranges from 0 to 1, is represented by the vertical axis. The diagram indicates that for the majority of the data, the suggested approach is more accurate than the other methods in every evaluation point.

The proposed method has been compared with SVM, Neural Network, Correlation, Euclidean, Differential, and Block (8x8) Differential methods in Fig. 17. The second scenario is the TP ratio diagram, which is the green colour of the proposed method, the red colour of Euclidean, the black colour of correlation, the blue colour of the support vector machine, the purple colour of the neural network, the blue colour of block 8x8, and the black colour of differential. In this case, the vertical axis is a percentage, while the horizontal axis represents the trained data % in the dataset. The suggested technique outperforms the other methods in all evaluation points for the majority of the data, as shown by the diagram.

The proposed method is compared with SVM, Neural Network, Correlation, and Euclidean methods in Fig. 18. The third scenario is the precision diagram, where the green colour represents the suggested method, the red colour represents the Euclidean method, the black colour represents a correlation, the blue colour represents a support vector machine, and the purple colour represents a neural network. In this case, precision is the vertical axis and the trained data percentage in the dataset is the horizontal axis. The diagram indicates that for the majority of the data, the recommended approach has outperformed alternative methods in every evaluation point.

The F-measure diagram, which compares the suggested method with the SVM, Neural Network, and Correlation methods in Fig. 20, represents the fifth scenario and Fig. 19 shows the recall diagram. It is coloured red for the proposed method, red for the correlation, blue for the support vector machine, and black for the neural network. The trained data % in the dataset is the horizontal axis in this case, and the f-measure percentage rate is the vertical axis. The diagram indicates that for the majority of the data, the recommended approach has a higher f-measure than the other methods in every evaluation point.

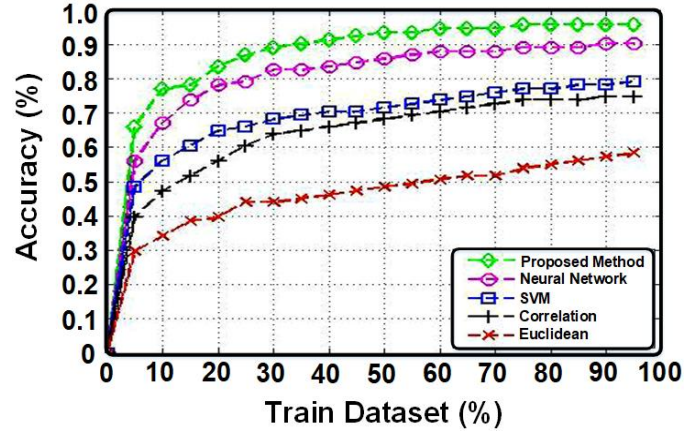


Fig. 16. Accuracy diagram.

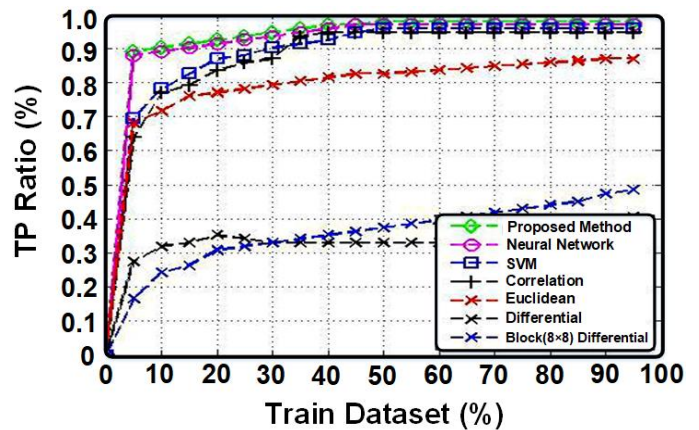


Fig. 17. TP Ratio.

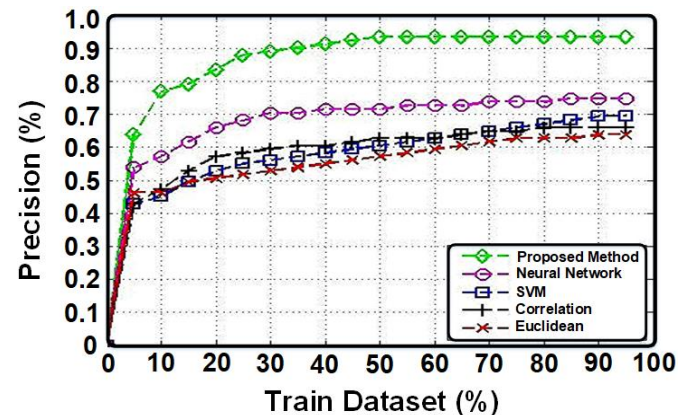


Fig. 18. Precision diagram.

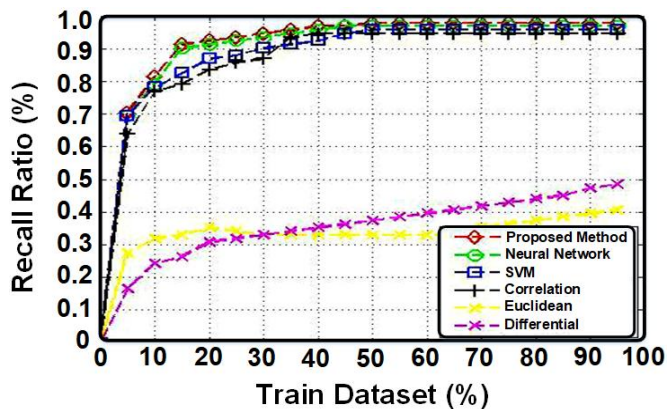


Fig. 19. Recall diagram.

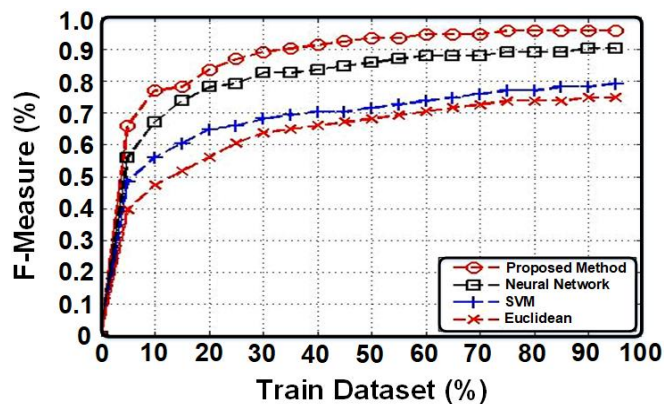


Fig. 20. F-measure diagram.

The sixth scenario, which contrasts the suggested technique with SVM and neural network methods in Fig. 21, shows the precision total diagram with the red colour of the suggested method, the black colour of the neural network, and the blue colour of the support vector machine.

In this case, the vertical axis represents the overall accuracy % while the horizontal axis represents the percentage of trained data in the dataset. The diagram indicates that for the majority of the data, the recommended approach has outperformed alternative methods in every evaluation point.

2) *Negatives evaluation results:* The seven sonorities are the total accuracy chart, which contrasts the red, green, blue, and black colours of the neural network, support vector machine, and SVM in the proposed method with the neural network and correlation methods in Fig. 22. The training data % in the dataset is shown by the horizontal axis in this example, while the total correctness percentage is represented by the vertical axis. The diagram indicates that for the majority of the data, the suggested approach is more accurate than alternative methods in all evaluation points.

Scenario eight involves the TN Ratio chart, which displays a comparison between the green colour representing the proposed method, the red colour representing correlation, the blue colour representing the neural network, and the black colour representing the support vector machine. This comparison is made with the SVM, Neural Network, and

Correlation methods, as shown in Fig. 23. The horizontal axis represents the percentage of trained data in the data set, while the vertical axis represents the ratio of true negatives (TN). Based on the diagram, the suggested technique exhibits a higher TN Ratio compared to other methods at all evaluation points for the majority of the data.

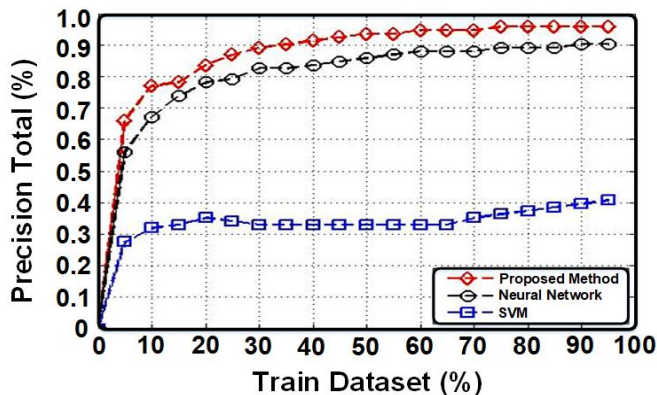


Fig. 21. Precision total diagram.

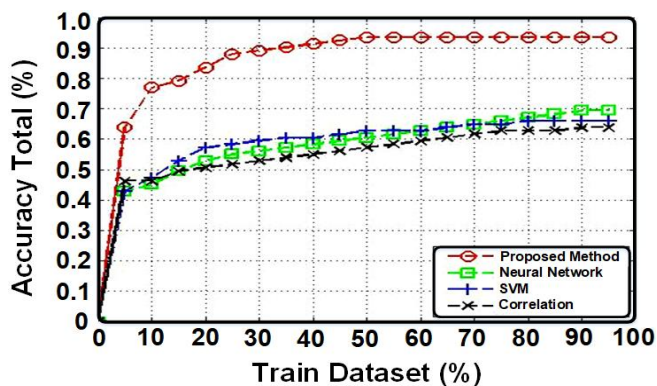


Fig. 22. Accuracy total diagram.

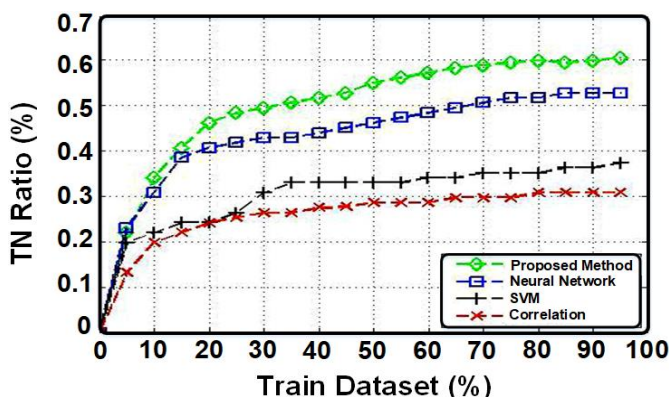


Fig. 23. TN Ratio diagram.

The precision TN diagram, which is coloured as follows: green for the suggested approach, red for Euclidean, black for the differential, blue for the support vector machine, and purple for the neural network, represents the ninth case. In Fig. 24, the suggested approach correlation is contrasted with the Differential, SVM, Euclidean, Neural Network, Correlation, and Block (8×8) Differential methods, as indicated by the black colour. In this case, the vertical axis represents the

percentage of TN accuracy, and the horizontal axis represents the proportion of trained data in the dataset. The suggested method outperforms competing methods in all evaluation points for the majority of the data, as shown by the chart.

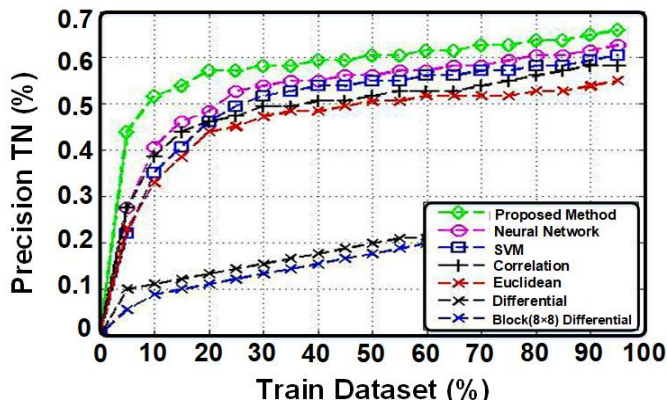


Fig. 24. Precision TN diagram.

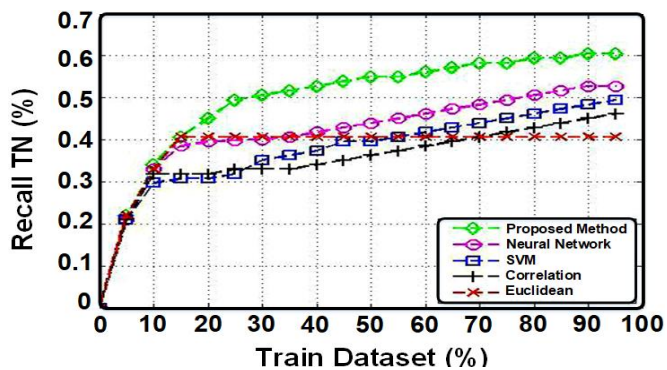


Fig. 25. Recall the TN diagram.

In Fig. 25, the Recall TN diagram presents a comparison between the proposed method and other methods, namely Euclidean, correlation, support vector machine (SVM), and neural network. The proposed method is represented by the green colour, Euclidean by red, correlation by black, SVM by blue, and neural network by purple. The horizontal axis represents the percentage of training data in the dataset, while the vertical axis represents the percentage of Recall TN. Based on the chart, the suggested technique exhibits higher Recall TN values compared to other methods across all evaluation points for the majority of the data.

The 11th scenario presents the TN accuracy diagram, where the proposed method is represented by black, Euclidean by red, correlation by black, support vector machine by red, neural network by blue, and differential by yellow. This diagram compares the proposed method with SVM, Neural Network, Correlation, and Euclidean methods. Fig. 26 presents a comparison of the differential. The horizontal axis represents the percentage of learned data in the dataset, while the vertical axis represents the accuracy rate of True Negative (TN). Based on the diagram, the suggested method demonstrates superior accuracy in true negatives (TN) compared to other methods across all evaluation points for the majority of the data.

Scenario twelve involves the comparison of the proposed technique, support vector machine (SVM), and neural network

using the F-measure TN diagram. The proposed method is represented by the colour purple, SVM by black and neural network by red. This comparison is depicted in Fig. 27. The horizontal axis in this scenario represents the percentage of trained data in the dataset, while the vertical axis represents the F-Measure TN. Based on the diagram; the suggested method consistently outperforms other methods in terms of F-Measure TN across all evaluation points for the majority of the data.

The performance of the suggested technique has been evaluated by comparing it with SVM, Neural Network, Correlation, Euclidean, Differential, and Block (8x8) Differential methods. The techniques are executed within the MATLAB simulation environment. The criteria of accuracy, precision, and sensitivity have been chosen for comparison and suggested for evaluating the approaches. The evaluation findings have been graphically shown and demonstrate that the suggested method outperforms previous methods in terms of accuracy, precision, sensitivity, and recall in all scenarios.

Table IV presents a comparison of distinct datasets that utilise various approaches with fused segmented images. The image datasets undergo pre-processing using image fusion methodology and are subsequently segmented using U-Net. Conversely, the method of merging images is not employed; just the segmentation of images is performed. It is evident that the techniques employed with fused images yield output that is comparable to that of non-fused images. The image fusion approach involves combining images obtained from diverse sensors, which contain essential data, using various numerical models to get a unified composite image.

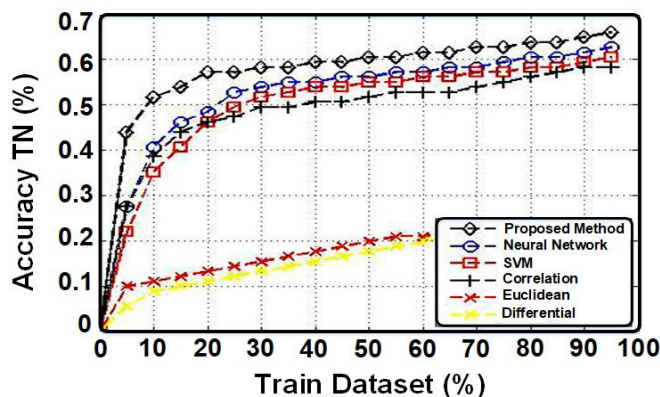


Fig. 26. Accuracy TN diagram.

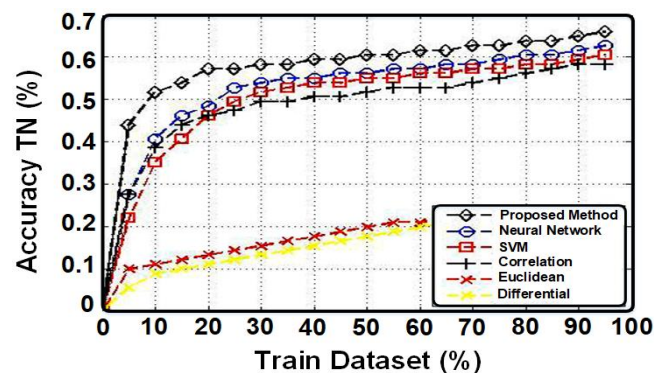


Fig. 27. F-measure TN diagram.

TABLE IV. COMPARATIVE ANALYSIS OF DIFFERENT PARAMETERS IN TERMS OF BRAIN TISSUE REGION IDENTIFICATION AND CLASSIFICATION USING MULTIMODAL IMAGING METHODS

Image Fusion	Image Segmentation Method	Classification Method	Dataset	Data Volume	Data Class	Accuracy (%)
Non-Fused Image	U-Net	U-Net	Brain tumour fig share	3074	3	96.21
Fused Image	U-Net	ResNet50	BraTS 2012	3074	3	95.34
Fused Image	U-Net	U-Net	BraTS 2018	3074	3	89.37
Fused Image	U-Net	CNN	BraTS 2018	3074	3	90.01
Non-Fused Image	U-Net	U-Net	BraTS 2012	3074	3	97.68
Fused Image	U-Net	ResNet50	BraTS 2012	3074	3	88.69
			Dataset Figshare	3074	3	98.71

## VI. CONCLUSION

This article presents a neural network-based method for automatically detecting brain tumours. Various methodologies are being examined. The evaluation method presents the results based on accuracy, precision, and sensitivity. The initial step involves presenting the pre-processing outcomes, encompassing histogram equalisation, median filtering, edge detection, binarization, and identification of related pixels. Subsequently, the detection outcomes for 766 data points are presented, with 14 of them being displayed. Subsequently, the evaluation relationships are articulated with respect to accuracy, correctness, and evaluation standards. Ultimately, the evaluation outcomes for the positives and the evaluation outcomes for the negatives are disclosed. The simulation is conducted with 766 data points, and the assessment criteria are also assessed. The proposed strategy for improvement is the utilisation of deep learning, which has enhanced the effectiveness of the previous method. The accuracy of these is verified, and subsequently, the detection approach is established and compared to alternative methodologies. In future research, it is possible to employ optimisation methods like as genetic algorithms and colonial competition, among others, in the field of deep learning as alternatives to the modified neural network.

## REFERENCES

- [1] T. Logeswari and M. Karnan, "An improved implementation of brain tumor detection using segmentation based on hierarchical self-organizing map," *International Journal of Computer Theory and Engineering*, vol. 2, no. 4, p. 591, 2010.
- [2] S. Agrawal, R. Panda, and L. Dora, "A study on fuzzy clustering for magnetic resonance brain image segmentation using soft computing approaches," *Appl Soft Comput*, vol. 24, pp. 522–533, 2014.
- [3] N. Gordillo, E. Montseny, and P. Sobrevilla, "State of the art survey on MRI brain tumor segmentation," *Magn Reson Imaging*, vol. 31, no. 8, pp. 1426–1438, 2013.
- [4] J. Liu, M. Li, J. Wang, F. Wu, T. Liu, and Y. Pan, "A survey of MRI-based brain tumor segmentation methods," *Tsinghua Sci Technol*, vol. 19, no. 6, pp. 578–595, 2014.
- [5] M. Prastawa, E. Bullitt, S. Ho, and G. Gerig, "A brain tumor segmentation framework based on outlier detection," *Med Image Anal*, vol. 8, no. 3, pp. 275–283, 2004.
- [6] N. Moon, E. Bullitt, K. Van Leemput, and G. Gerig, "Automatic brain and tumor segmentation," in *Medical Image Computing and Computer-Assisted Intervention—MICCAI 2002: 5th International Conference Tokyo, Japan, September 25–28, 2002 Proceedings, Part I 5*, Springer, 2002, pp. 372–379.
- [7] B. H. Menze, K. Van Leemput, D. Lashkari, M.-A. Weber, N. Ayache, and P. Golland, "A generative model for brain tumor segmentation in multi-modal images," in *Medical Image Computing and Computer-Assisted Intervention—MICCAI 2010: 13th International Conference, Beijing, China, September 20–24, 2010, Proceedings, Part II 13*, Springer, 2010, pp. 151–159.
- [8] D. Kwon, R. T. Shinohara, H. Akbari, and C. Davatzikos, "Combining generative models for multifocal glioma segmentation and registration," in *Medical Image Computing and Computer-Assisted Intervention—MICCAI 2014: 17th International Conference, Boston, MA, USA, September 14–18, 2014, Proceedings, Part I 17*, Springer, 2014, pp. 763–770.
- [9] M. K. Abd-Elilah, A. I. Awad, A. A. M. Khalaf, and H. F. A. Hamed, "A review on brain tumor diagnosis from MRI images: Practical implications, key achievements, and lessons learned," *Magn Reson Imaging*, vol. 61, pp. 300–318, 2019.
- [10] Zhao, Y., Liang, H., Zong, G., & Wang, H. (2023). Event-Based Distributed Finite-Horizon  $H_\infty$  Consensus Control for Constrained Nonlinear Multiagent Systems. *IEEE Systems Journal*.
- [11] G. Mohan and M. M. Subashini, "MRI based medical image analysis: Survey on brain tumor grade classification," *Biomed Signal Process Control*, vol. 39, pp. 139–161, 2018.
- [12] Bilbas, H., & Kadir, D. H. (2019). An application of factor analysis to identify the most effective reasons that university students hate to read books. *International Journal of Innovation, Creativity and Change*, 6(2), 251–265.
- [13] Samiei, M., Hassani, A., Sarspy, S., Komari, I. E., Trik, M., & Hassanpour, F. (2023). Classification of skin cancer stages using a AHP fuzzy technique within the context of big data healthcare. *Journal of Cancer Research and Clinical Oncology*, 1–15.
- [14] Cheng, F., Niu, B., Xu, N., Zhao, X., & Ahmad, A. M. (2023). Fault detection and performance recovery design with deferred actuator replacement via a low-computation method. *IEEE Transactions on Automation Science and Engineering*.
- [15] Cao, C., Wang, J., Kwok, D., Cui, F., Zhang, Z., Zhao, D., ... & Zou, Q. (2022). webTWAS: a resource for disease candidate susceptibility genes identified by transcriptome-wide association study. *Nucleic acids research*, 50(D1), D1123–D1130.
- [16] N. Le Roux and Y. Bengio, "Representational power of restricted Boltzmann machines and deep belief networks," *Neural Comput*, vol. 20, no. 6, pp. 1631–1649, 2008.
- [17] Xiao, L., Cao, Y., Gai, Y., Khezri, E., Liu, J., & Yang, M. (2023). Recognizing sports activities from video frames using deformable convolution and adaptive multiscale features. *Journal of Cloud Computing*, 12(1), 1–20.
- [18] Sajadi, S. M., Kadir, D. H., Balaky, S. M., & Perot, E. M. (2021). An Eco-friendly nanocatalyst for removal of some poisonous environmental pollutants and statistically evaluation of its performance. *Surfaces and Interfaces*, 23, 100908.
- [19] A. Hyvärinen and P. Hoyer, "Emergence of phase-and shift-invariant features by decomposition of natural images into independent feature subspaces," *Neural Comput*, vol. 12, no. 7, pp. 1705–1720, 2000.

- [20] Sun, J., Zhang, Y., & Trik, M. (2022). PBPHS: a profile-based predictive handover strategy for 5G networks. *Cybernetics and Systems*, 1-22.
- [21] Trik, M., Akhavan, H., Bidgoli, A. M., Molk, A. M. N. G., Vashani, H., & Mozaffari, S. P. (2023). A new adaptive selection strategy for reducing latency in networks on chip. *Integration*, 89, 9-24.
- [22] Omer, A. W., Blbas, H. T., & Kadir, D. H. (2021). A Comparison between Brown's and Holt's Double Exponential Smoothing for Forecasting Applied Generation Electrical Energies in Kurdistan Region.
- [23] Wang, G., Wu, J., & Trik, M. (2023). A Novel Approach to Reduce Video Traffic Based on Understanding User Demand and D2D Communication in 5G Networks. *IETE Journal of Research*, 1-17.
- [24] Kadir, D. H. (2021). Statistical evaluation of main extraction parameters in twenty plant extracts for obtaining their optimum total phenolic content and its relation to antioxidant and antibacterial activities. *Food Science & Nutrition*, 9(7), 3491-3499.
- [25] Wang, Z., Jin, Z., Yang, Z., Zhao, W., & Trik, M. (2023). Increasing efficiency for routing in Internet of Things using Binary Gray Wolf Optimization and fuzzy logic. *Journal of King Saud University-Computer and Information Sciences*, 35(9), 101732.
- [26] Zhao, H., Zong, G., Zhao, X., Wang, H., Xu, N., & Zhao, N. (2023). Hierarchical Sliding-Mode Surface-Based Adaptive Critic Tracking Control for Nonlinear Multiplayer Zero-Sum Games Via Generalized Fuzzy Hyperbolic Models. *IEEE Transactions on Fuzzy Systems*.
- [27] B. Moradhasel, A. Sheikhan, O. Aloosh, and N. J. Dabanloo, "Spectrogram classification of patient chin electromyography based on deep learning: A novel method for accurate diagnosis obstructive sleep apnea," *Biomed Signal Process Control*, vol. 79, p. 104215, 2023.
- [28] Kadir, D. (2018). Bayesian inference of autoregressive models (Doctoral dissertation, University of Sheffield).
- [29] Ding, X., Yao, R., & Khezri, E. (2023). An efficient algorithm for optimal route node sensing in smart tourism Urban traffic based on priority constraints. *Wireless Networks*, 1-18.
- [30] Zhao, H., Zong, G., Wang, H., Zhao, X., & Xu, N. (2023). Zero-Sum Game-Based Hierarchical Sliding-Mode Fault-Tolerant Tracking Control for Interconnected Nonlinear Systems via Adaptive Critic Design. *IEEE Transactions on Automation Science and Engineering*.
- [31] Fakhri, P. S., Asghari, O., Sarspy, S., Marand, M. B., Moshaver, P., & Trik, M. (2023). A fuzzy decision-making system for video tracking with multiple objects in non-stationary conditions. *Heliyon*.
- [32] Zhang, H., Zou, Q., Ju, Y., Song, C., & Chen, D. (2022). Distance-based support vector machine to predict DNA N6-methyladenine modification. *Current Bioinformatics*, 17(5), 473-482.
- [33] Saleh, D. M., Kadir, D. H., & Jamil, D. I. (2023). A Comparison between Some Penalized Methods for Estimating Parameters: Simulation Study. *QALAAI ZANIST JOURNAL*, 8(1), 1122-1134.
- [34] Xue, B., Yang, Q., Jin, Y., Zhu, Q., Lan, J., Lin, Y., ... & Zhou, X. (2023). Genotoxicity Assessment of Haloacetaldehyde Disinfection Byproducts via a Simplified Yeast-Based Toxicogenomics Assay. *Environmental Science & Technology*, 57(44), 16823-16833.
- [35] S. Xie, R. Girshick, P. Dollár, Z. Tu, and K. He, "Aggregated residual transformations for deep neural networks," in *Proceedings of the IEEE conference on computer vision and pattern recognition*, 2017, pp. 1492–1500.
- [36] A. Achille and S. Soatto, "Emergence of invariance and disentanglement in deep representations," *The Journal of Machine Learning Research*, vol. 19, no. 1, pp. 1947–1980, 2018.
- [37] Pitchai, R., Supraja, P., Victoria, A. H., & Madhavi, M. J. N. P. L. (2021). Brain tumor segmentation using deep learning and fuzzy K-means clustering for magnetic resonance images. *Neural Processing Letters*, 53, 2519-2532.
- [38] VK, D. (2023). An intelligent brain tumor segmentation using improved Deep Learning Model Based on Cascade Regression method. *Multimedia Tools and Applications*, 82(13), 20059-20078.